Published as: *Cell*. 2007 December 28; 131(7): 1313–1326.

Architecture of a Coat for the Nuclear Pore Membrane

Kuo-Chiang Hsia, **Pete Stavropoulos**, **Günter Blobel***, and **André Hoelz***
Laboratory of Cell Biology, Howard Hughes Medical Institute, The Rockefeller University, 1230 York Avenue, New York, NY 10021, USA

SUMMARY

The symmetric core of the nuclear pore complex can be considered schematically as a series of concentric cylinders. A peripheral cylinder coating the pore membrane contains the previously characterized, elongated heptamer that harbors Sec13-Nup145C in its middle section. Strikingly, Sec13-Nup145C crystallized as a hetero-octamer in two space groups. Oligomerization of Sec13-Nup145C was confirmed biochemically. Importantly, the numerous interacting surfaces in the hetero-octamer are evolutionarily highly conserved, further underlining the physiological relevance of the oligomerization. The hetero-octamer forms a slightly curved, yet rigid rod of sufficient length to span the entire height of the proposed membrane-adjacent cylinder. In concordance with the dimensions and symmetry of the nuclear pore complex core, we suggest that the cylinder is constructed of four anti-parallel rings, each ring being composed of eight heptamers arranged in a head-to-tail fashion. Our model proposes that the hetero-octamer would vertically traverse and connect the four stacked rings.

INTRODUCTION

The nuclear pore complex (NPC) mediates the selective exchange of macromolecules between the nucleus and cytoplasm (Hoelz and Blobel, 2004; Pemberton and Paschal, 2005). Electron microscopic reconstructions have revealed that the NPC is a cylindrical structure that consists of a central core with eight-fold rotational symmetry across a nucleo-cytoplasmic axis and two-fold symmetry in the plane of the nuclear envelope (Beck et al., 2004; Yang et al., 1998). This symmetric core is linked to asymmetric “cytoplasmic filaments” and a “nuclear basket” structure (Fahrenkrog et al., 2004). The NPC is one of the largest supramolecular assemblies in the eukaryotic cell (Reichelt et al., 1990), composed of about 30 different proteins termed nucleoporins (nups) (Cronshaw et al., 2002; Rout et al., 2000). In cells with open mitosis, the NPC is disassembled either into individual nups or various nup sub-complexes (Belgareh et al., 2001; Glavy et al., 2007; Loiodice et al., 2004; Vasu et al., 2001). Similar sub-complexes have also been obtained by dissecting intact NPCs using non-ionic detergents and a range of salt concentrations (for review see Suntharalingam and Wente, 2003).

In yeast, *in vivo* dissection employing the tagging of proteins and subsequent pullout initially yielded a pentameric “Nup84” complex consisting of Nup84, Nup120, Nup85, Sec13, and Seh1 (Siniossoglou et al., 1996). Subsequent pullout experiments established that Nup145C and Nup133 are additional members of a now heptameric Nup84 complex (Allen et al., 2001;

*Correspondence: hoelza@rockefeller.edu (A.H.), blobel@rockefeller.edu (G.B.).

Accession Numbers
The atomic coordinates of the monoclinic and orthorhombic structures have been deposited to the Protein Data Bank with the accession codes 3BG0 and 3BG1.

Lutzmann et al., 2005; Siniossoglou et al., 2000). To reconstitute the heptameric Nup84 complex from recombinant yeast proteins, Lutzmann et al. co-expressed up to three tagged nups in *Escherichia coli*, purified the resulting complexes, and assembled them into a heptamer (Lutzmann et al., 2002). By subjecting the individual sub-complexes and the assembled heptamer to shape analysis by negative stain electron microscopy, the relative position of the seven members within the heptamer could be established (Figure 1A). Nup133 is at the base, followed by Nup84, the Sec13-Nup145C complex in the center, and the Nup120-Nup85-Seh1 complex at the top. Nup120 is capable of interacting with both the Sec13-Nup145C, as well as with the Seh1-Nup85 complex. The entire heptamer measures about 400 Å in length and forms a Y-shaped structure.

Although the spatial arrangement of the heptameric complexes in the symmetric NPC core is currently unknown, it has been suggested that they serve as “membrane-curving modules”, similar to the members of the COPI, COPII, and clathrin complexes (Devos et al., 2004). The heptameric complex may “coat” the curvature between the inner and outer nuclear membrane (also termed the “pore membrane” domain of the nuclear envelope, or POM). Intriguingly, Sec13 is not only a member of the NPC, but also of the COPII complex (Bickford et al., 2004; Fath et al., 2007; Gurkan et al., 2006; Lederkremer et al., 2001; Salama et al., 1997). In addition, Nup133 has been shown to contain a membrane-curvature-sensing motif, further supporting the nuclear pore membrane localization of the heptamer within the NPC (Drin et al., 2007).

All members of the yeast heptameric complex are evolutionarily conserved, but the vertebrate counterpart contains two additional proteins, Nup43 and Nup37 (Fontoura et al., 1999; Glavy et al., 2007; Loiodice et al., 2004; Vasu et al., 2001; Walther et al., 2003). Deletion or immunodepletion of any nup from these complexes in yeast or other eukaryotic cells has dramatic consequences on the organization of the nuclear envelope and the NPC, as well as on the nuclear export of polyadenylated RNAs (Bai et al., 2004; Boehmer et al., 2003; Dockendorff et al., 1997; Siniossoglou et al., 1996; Siniossoglou et al., 2000; Vasu et al., 2001).

The proteins of the heptameric complex have been predicted to be β-propellers (Sec13, Seh1), α-helical solenoids (Nup84, Nup85, Nup145C), or a combination of both (Nup133, Nup120) (Devos et al., 2006). To date, the only domain of the heptameric complex for which an atomic structure has been determined is the β-propeller domain of Nup133 (Berke et al., 2004). Here, we report the biochemical characterization and the crystal structure of the hetero-dimeric Sec13-Nup145C complex. Based on our present structural analysis and previous electron microscopical studies, we propose a model depicting how the heptameric complex is organized into a cylindrical, membrane-coating scaffold in the NPC.

RESULTS

Analysis of Oligomeric State

Nup145C is generated by the autoproteolytic cleavage of a nascent precursor polypeptide, yielding Nup145N and Nup145C (Nup98 and Nup96 in vertebrates) (Fontoura et al., 1999; Teixeira et al., 1997). The yeast Nup145C polypeptide chain (residues 1 to 711) can be divided into two regions: an N-terminal, 125 residue region which lacks any apparent structural elements followed by a 586 residue region which is predominantly α-helical and which has been predicted to form an α-helical solenoid domain (Figure 1B). Both human and yeast Sec13 contain six WD40 repeats which form a β-propeller (Fath et al., 2007; Saxena et al., 1996) (Figure 1B). Interestingly, the human Sec13 contains an additional C-terminal region of 25 residues that is not present in the yeast homologue.

We designed a large array of constructs of ySec13, hSec13, and yNup145C and co-expressed them as recombinant proteins to obtain isomeric yeast-yeast or chimeric human-yeast Sec13-Nup145C complexes. The resulting complexes were characterized by limited proteolysis (Figure S1). We found a proteolytically stable fragment of Nup145C (residues 125 to 555) that was used in all subsequent experiments and, for the sake of simplicity, is referred to as Nup145C. For ySec13, full-length constructs were used exclusively, whereas for hSec13 either full-length or a C-terminally truncated form (residues 1 to 316) were employed. The resulting isomeric or chimeric dimers were then analyzed by size-exclusion chromatography (SEC).

Sec13-Nup145C hetero-dimers that contained either yeast (Figure 1C) or human (Figure 1D) full-length Sec13 formed higher order oligomers in a concentration-dependent fashion. Various oligomerization states were observed. There was a dynamic equilibrium between hetero-dimeric and hetero-tetrameric states in the yeast-yeast complex, with a small amount of hetero-octamers observed at high concentrations (Figure 1C). Likewise, there was a dynamic equilibrium between hetero-dimeric and hetero-tetrameric states for the chimeric human-yeast complex, although a higher ratio of hetero-octamer and even an additional hetero-dodecamer peak existed (Figure 1D). In conclusion, both isomeric and chimeric Sec13-Nup145C hetero-dimers resemble each other in their tendency to oligomerize.

We obtained crystals from isomeric and chimeric hetero-dimers that contained full-length Sec13, but they were of low crystallographic quality. We discovered that truncation of hSec13 by six residues yielded higher quality crystals. We refer to this complex of truncated proteins as the Sec13-Nup145C hetero-dimer.

SEC of this chimeric complex showed again a dynamic equilibrium between hetero-dimers and hetero-tetramers. However, the reduced oligomerization tendency of this chimeric complex yielded only barely detectable amounts of hetero-octamers (Figure 1E). Further analysis of the principal peak of the chimeric hetero-dimer by combining SEC with multiple angle light scattering (Figure 1F) unambiguously established that the peak in Figure 1E represents a dynamic equilibrium between hetero-dimers and hetero-tetramers.

We also analyzed the oligomeric behavior of human and yeast Sec13 in isolation by SEC and found that both proteins exist in a dynamic equilibrium between monomers and dimers (Figure S2A, B). The much higher degree of hSec13 dimerization is strongly dependent on the final six C-terminal residues (Figure S2C).

Structure Determination

Crystals of the Sec13-Nup145C hetero-dimer appeared in the monoclinic space group C2 and the orthorhombic space group $C222_1$. Each crystal form contained an identical ~400 kDa hetero-octamer in the asymmetric unit. The structures of both crystal forms were determined independently by multiple anomalous dispersion (MAD), using X-ray diffraction data obtained from seleno-L-methionine (SeMet)-labeled and several heavy-metal derivatized crystals (Figure S3). The final structures derived from the two space groups were refined to a 3.0 Å and 3.15 Å resolution, respectively (for details see Tables S1 and S2). As the two structures are overall very similar, we will focus our discussion on the structural information obtained from the orthorhombic crystal form.

Architectural Overview

The Sec13-Nup145C hetero-octamer forms a slightly bent rod with overall dimensions of approximately 285 Å × 100 Å × 50 Å (Figures 2A, B, and Movies S1, S2). The rod contains three pseudo-two-fold axes of symmetry. The central axis of symmetry passes through two hetero-tetramers that associate primarily, but not exclusively, via the homo-dimerization of

Sec13. Around the adjacent two axes of symmetry, hetero-dimers interact exclusively through the homo-dimerization of Nup145C.

Both Sec13 and Nup145C interact with each other via several distinct surfaces that have been highly conserved in evolution. Overall, Nup145C has a novel fold in the form of a U-shaped structure (Figure 3A). Sec13 contains six WD40 repeats that fold into an "open", six-bladed β-propeller. In contrast to a canonical β-propeller fold, there is no "Velcro" closure. The N-terminal domain of Nup145C forms an additional three-stranded blade that is inserted into Sec13's β-propeller fold, complementing it with a seventh blade (Figures 3B–E, and Movies S3, S4).

Structure of the Sec13-Nup145C Hetero-Dimer

Our Sec13 expression construct contains 14 residues on its N-terminus that are predicted to contain an additional β-strand that would typically complete the last blade in the β-propeller architecture, as well as 12 C-terminal residues that are predicted to contain two additional β-strands. However, these residues are not visible in the electron density map and therefore are presumably disordered. Hence, we detected the C-terminal residues that are common for ySec13 and hSec13, but not the additional C-terminal residues that are unique to hSec13.

The ~50 residue N-terminal region of Nup145C folds into an α-helix (αA), followed by a short connecting segment (αA-β1 connector), and three anti-parallel β-strands (β1-β3) (Figure 3A). Together, this region represents the "domain invasion motif", or DIM, of Nup145C. The DIM's α-helix αA and the αA-β1 connector segment interact with Sec13's D-A and B-C loops from all six of its blades, forming the top face of the β-propeller domain (Figures 3B–E). These surface loops form a circular bracelet that appears to stabilize the open conformation of Sec13's β-propeller domain. The DIM's three β-strands form a seventh blade that is inserted between blades 1 and 6 of the Sec13 β-propeller domain (Figures 3D, E).

The DIM is followed by a short segment that connects an ~400 residue C-terminal domain. This C-terminal domain is principally constructed of 18 anti-parallel α-helices (αB-αS) that form a novel fold (Figure 3A). A striking kink extending from αE to αH allows the chain to fold back onto itself. The resulting U-shaped structure is held together by extensive hydrophobic interactions between the ascending and descending arms of the "U" and by a 20 residue long loop (between αB and αC) that extends from the U's descending arm and wraps around the U's ascending arm (Figures 3A–C). The four C-terminal α-helices (αP-αS) tightly interact with almost all of the A-B and C-D loops of the six blades that connect the β-strands on the bottom face of Sec13's β-propeller domain (Figure 3B). Altogether, the interaction between the two proteins covers ~5,250 $Å^2$ of surface area and involves 69 and 58 residues of Sec13 and Nup145C, respectively (Figures S4–S7). The Sec13 residues participating in complex formation are essentially conserved between human and yeast, in line with the observation that human Sec13 can replace yeast Sec13 in the Sec13-Nup145C complex (Figure S1). The conservation, the nature, and the sheer size of the Nup145C and Sec13 interaction strongly suggest that both proteins form a very tight structural unit, highly conserved through eukaryotic evolution.

Structure of the Sec13-Nup145C Hetero-Tetramer

The hetero-tetramer is formed by head-to-head homo-dimerization of Nup145C. Four α-helices (αF, αH, αI, and αJ) that are located in the center of the domain at the sharp kink where the domain folds back onto itself form a predominantly hydrophobic interface that covers ~2,700 $Å^2$ of surface area (Figure 4). A two-fold axis of symmetry runs through the dimerization interface (Figure 5A). Again, this interface is highly conserved and appears to stabilize the sharp kink of the Nup145C α-helical domain.

The Curved Hetero-Octameric Sec13-Nup145C Rod

In both crystal forms, we identified identical Sec13-Nup145C hetero-octamers that are packed differently in the two crystal lattices. These two hetero-octamers superimpose with a mean square root deviation of 0.75 Å, strongly suggesting that the overall structure is rigid (Figure S8). The hetero-octamer is constructed by the head-to-head interaction of two hetero-tetramers, involving the surfaces of both Sec13 and Nup145C. Yet again, the two interacting interfaces are highly conserved in evolution and are predominantly hydrophobic (Figures 4). The first interface is via Sec13 homo-dimerization and is facilitated by the two terminal β-strands C and D of blades 5 and 6, the inter-blade groove between the two blades, as well as the connector loops 5D-6A and 6BC (Figure 5B). This interface covers ~1,100 $Å^2$ of surface area buried between the two Sec13 β-propellers. The Sec13 dimerization surface is essentially invariant between the yeast and human proteins (Figures S4 and S6). The second interface is generated by the *trans* interaction of each of the two Sec13 β-propellers with an adjacent Nup145C. This interaction involves the inter-blade connector loops 3D-4A and 4D-5A of Sec13 and the αM-αN connector loop of the Nup145C α-helical domain and together covers 600 $Å^2$. Hence, in total, ~1,700 $Å^2$ of surface area is buried between the two Sec13-Nup145C hetero-tetramers (Figure 4 and Figure S7).

The fact that we crystallized a hetero-octamer, when this form was present in solution only in small quantities, is readily explained by protein concentration differences that we estimate to be more than one order of magnitude higher in the crystal than the highest concentration we tested in solution (Figure 1). A protein concentration similar to that in the crystal is likely in the NPC *in vivo*.

In conclusion, the architecture of the hetero-octamer is shaped by multiple interactions involving several interfaces. The highly conserved interfaces exhibit a scale of strength that is based on their character and size. This is also confirmed by our solution data and by the PISA interface evaluation algorithm (Krissinel and Henrick, 2005).

A Conserved Architectural Principle

Within the NPC, Sec13 has a close homolog, Sec13-homology-1 (Seh1), that is associated with Nup85. The Seh1-Nup85 hetero-dimer is located at one end of the heptameric complex (Lutzmann et al., 2002). Sec13 and Seh1 share ~70 % homology on the sequence level. Of the 37 Sec13 residues that are directly involved in the formation of the $Nup145C^{DIM}$ interface, 20 residues are identical, and 17 residues are conserved in Seh1 (Figure S4). This analysis strongly suggests that the Seh1 β-propeller domain forms an identical overall structure. Moreover, Nup145C and Nup85 are similar in size and share an identical domain structure, in which a short N-terminal β-sheet region is followed by a C-terminal α-helical domain. Although the overall sequence homology between Nup145C and Nup85 is only ~35 %, both proteins can be aligned (Figure S5), suggesting that the two proteins form the same overall fold. Through secondary structure analysis, the N-terminal region of Nup85 is predicted to form a short N-terminal α-helix followed by three short β-strands. This arrangement closely resembles the secondary structures of the DIMs of Nup145C and Nup96 (the human homolog of Nup145C), suggesting that Nup85 contains a DIM that is capable of complementing the β-propeller fold of Seh1 (Figure S9). Strikingly, the most highly conserved Nup85 residues are located in the α-helices that form the homo-dimerization element of the Nup145C α-helical domain, suggesting that Nup85 is also capable of dimerizing.

To test this prediction, we expressed a yeast-yeast Seh1-Nup85 hetero-dimer using full-length Seh1 and a fragment of Nup85 containing residues 1 to 570. The design of this Nup85 fragment was based on the Nup145C and Nup85 sequence alignment (Figure S5). The expressed Seh1-Nup85 complex was purified and analyzed by SEC. We found that the Seh1-Nup85 complex

forms a dynamic equilibrium between hetero-tetramers and hetero-octamers (Figure 6), very similar to the Sec13-Nup145C complex (Figure 1). In contrast to the Sec13-Nup145C, the Seh1-Nup85 dimers are tightly associated, yielding a sharp hetero-tetramer peak even at lower concentrations, with no hetero-dimers detectable (Figure 6). Hence, the two complexes differ only in the relative strengths of their tetramerization interfaces, confirming our prediction that these two complexes are likely to be structurally similar.

DISCUSSION

We have determined the crystal structure of the Sec13-Nup145C dimer, a centrally located part of a previously characterized heptameric sub-complex of the NPC. Most strikingly, Sec13-Nup145C forms a hetero-octamer in two independent crystal forms as well as in solution. These data led us to propose a model of how this hetero-octamer organizes heptameric sub-complexes into a peripheral cylindrical scaffold coating of the pore membrane of the nuclear envelope (Figure 7).

Structure of the Sec13-Nup145C Hetero-Octamer

The key aspect of this model is our finding here, that Sec13-Nup145C forms a hetero-octamer (Figure 2). The basic unit of this structure is the Sec13-Nup145C hetero-dimer (Figure 3). The N-terminal portion of Nup145C invades the six-bladed β-propeller structure of Sec13, thereby providing a seventh blade. The remaining portion of Nup145C forms a domain of eighteen anti-parallel α-helices. A sharp kink in the middle of this α-helical domain results in an overall U-shaped structure (Figure 3). Next, the Sec13-Nup145C dimer forms a hetero-tetramer via a head-to-head association involving the bent region of the two Nup145Cs (Figure 2). Finally, two hetero-tetramers associate into a hetero-octamer via the homo-dimerization of Sec13 and the interaction of a Sec13 with the descending arm of the U of a “trans” Nup145C molecule (Figure 2, 5). We have also shown that Sec13 can form a dimer in solution (Figure S2), supporting the critical role that Sec13 plays in the hetero-octamerization.

The intermolecular interactions within the hetero-octamer involve large, primarily hydrophobic surfaces. Strikingly, all of these interfaces are evolutionarily highly conserved (Figure 4 and Figures S4–S7) and, therefore, are likely to be physiologically relevant. However, it remains to be established whether this hetero-octamer also exists *in vivo* and to what extent the presence of other nups would affect oligomerization.

Model for the Structural Function of Sec13-Nup145C as a Pole in a Pore Membrane Coat

Our discovery of the Sec13-Nup145C hetero-octamer and the elucidation of its structure yielded important insight about the architecture of the coat adjacent to the pore membrane of the nuclear envelope. Based on the order of the Sec13 and Nup145C molecules in the hetero-octamer and the fact that the hetero-octamer forms a bent rod about 285 Å long and with three approximately equidistant axes of two-fold symmetry (Figure 2), we propose that the hetero-octamer forms a vertical pole that connects four horizontally arranged rings, each composed of eight heptamers (Figure 7A, B). To satisfy the symmetry of the hetero-octamer, the heptamers in each ring must be arranged in a head-to-tail fashion (Figure 7A) and the rings stacked on top of each other in an anti-parallel manner (Figure 7B). Moreover, because the hetero-octamer is a slightly bent rod (Figure 2), we suggest that the concave surface of this rod follows the bent contour of the pore membrane, whereas the convex surface faces the next inward layer of nups. Our model satisfies the requirements for the outer dimension (about 1000 Å in diameter and 300 Å in height) and the axes of symmetry (eight-fold axis in the nucleo-cytoplasmic direction and a perpendicular two-fold axis in the plane of the nuclear envelope) of the symmetric core of the yeast NPC that were established by cryo-electron microscopy (Yang et al., 1998). Regarding various established dimensions, each heptamer has been

determined by negative stain electron microscopy to be about 400 Å long (Lutzmann et al., 2002). Hence, eight heptamers would add up to a ring of 3,200 Å circumference with a diameter of about 1000 Å. Furthermore, the length of the Sec13-Nup145C hetero-octamer of ~285 Å matches the height of the core of the NPC (Yang et al., 1998). With respect to symmetry, the two-fold axis of symmetry passing through the tetramerization interface (Figure 2) and the circumferential arrangement of eight heptamers in head-to-tail order in each of the rings (Figure 7B) satisfies the requirement for two-fold and eight-fold axes of symmetry, respectively.

A Seh1-Nup85 Hetero-Octamer May Function as an Additional Pole in the Pore Membrane Coat

Our finding that Nup85 is structurally homologous to Nup145C suggested that it may interact with Seh1 in a way similar to Sec13's interaction with Nup145C, i.e. that the N-terminal region of Nup85 may contribute a seventh blade to the six-bladed Seh1 β-propeller. Moreover, the C-terminal regions of Nup145C and Nup85 are conserved in their sequence and secondary structure, suggesting that they form a similar overall fold (Figure S5). Indeed, when we expressed the Seh1-Nup85 hetero-dimer with domain boundaries predicted by sequence alignments, we detected similar hetero-octameric assemblies by SEC (Figure 6). These data strongly support our model and suggest that Seh1-Nup85 forms a second vertical pole in the heptameric complex scaffold, yielding a total of 16 poles (Figure 7A, B). The two poles might be linked by their association with Nup120 and the Nup84-Nup133 hetero-dimer. Of course, our model leaves room for additional interactions of the heptameric nups in both the horizontal and vertical direction and, therefore, might be helpful in instructing a directed structural and biochemical analysis of the cylindrical scaffold.

Further Implication of the Model

Based on the slight curvature of the Sec13-Nup145C hetero-octamer, the cylindrical scaffold of the coat requires a wider circumference in the bottom and top rings of the cylinders. Closer inspection of the arrangement indicates the presence of unique sites in the bottom and top rings. For example, there are unpaired Sec13 dimerization surfaces as well as the heptameric head-to-tail sites that are present (or accessible) only in the top and bottom rings. These distinct marks could serve to direct the attachment and interdigitation of asymmetric nups, thereby perhaps also yielding a wider diameter of the outer rings.

Our model suggests a stoichiometry of 32 copies of each of the heptamer nups per NPC, with a total mass of approximately 16 megadaltons. This conclusion conflicts with previous estimates that were based on semi-quantitative methods and that suggested 16 copies of the heptameric nups per NPC (Cronshaw et al., 2002; Rout et al., 2000). It is clear, however, that these semi-quantitative determinations could only yield nup ratios but not absolute numbers.

We have also considered an alternative arrangement of the Sec13-Nup145C hetero-octamer, where the bent rod would be rotated: the long axis by 90°, placing it in the plane of the nuclear envelope, and the short axis by 180°, whe reby the convex surface would face the center of the pore. To satisfy the symmetry and the dimension of the NPC core, the hetero-octamer must further polymerize so as to obtain a closed ring with a diameter of ~1,000 Å. However, the hetero-octamer polymerization, primarily via Sec13 homo-dimerization (Figure S10A), yields a stretched-out spiral rather than a closed ring, with an outer diameter of only ~300 Å (Figure S10B). Furthermore, such an alternative arrangement is also not in agreement with our oligomerization data on the Seh1-Nup85 complex. Hence, this alternative arrangement is likely physiologically irrelevant.

Architecture of the NPC Core as a Series of Concentric Cylinders

In our highly schematic representation (Figure 7C), we have depicted the NPC core as a series of concentric cylinders. The innermost cylinder represents the conduit for nucleo-cytoplasmic transport and is envisaged to be composed of the α-helical domains of channel nups. An atomic structure of two α-helical domains of two representative channel nups has recently been established (Melcak et al., 2007). These nups contain "sliding" α-helices that may allow varying the diameter of the central transport cylinder according to cargo size. Because of the dynamic aspect of the components of the innermost transport cylinder, we envisage that the nups that are sandwiched between the transport and the coat cylinder would function as adapters, cushioning the dynamic variations in the transport cylinder diameter. Of course, the concept of a series of concentric cylinders should not be misinterpreted as meaning that these have "solid" walls. Rather, we envisage porous walls that would allow interdigitation and invasion of nup regions from adjacent cylinders. For example, the sixteen poles of the coat cylinder could form the poles of a fence, in which horizontal interconnections between domains of integral membrane proteins of the pore membrane cylinder and the adapter nup cylinder could be established. A great deal of flexibility in protein associations, both in the horizontal and vertical direction of these cylinders, must occur to accommodate the movement of the cytoplasmic/nucleoplasmic portions of integral membrane proteins across the NPC (King et al., 2006). Moreover, electron-tomographic studies reveal dynamics in the structure of the NPC induced by the transport of soluble substrates (Beck et al., 2004).

Comparison to COPII Complex

After completion of our crystallographic analyses, Fath et al. published crystal structures depicting the yeast Sec13-Sec31 hetero-dimer that is part of the COPII complex for vesicular transport from the ER to the Golgi apparatus (Fath et al., 2007). The only structural similarity between the Sec13-Nup145C and the Sec13-Sec31 hetero-dimers is that in both cases the dimerization partner provides a seventh blade to the Sec13 β-propeller. The hetero-dimer structure, the oligomerization to a hetero-tetramer, and the proposed higher order oligomerization of these two complexes are completely different (Figure S11).

The conserved feature between the two structures is the six-bladed Sec13 β-propeller domain that is complemented by an additional seventh blade provided by the DIMs of Nup145C or Sec31. Strikingly, the Sec13 β-propeller domain is capable of accommodating both DIMs even though they are completely different in their primary sequence (Figures S9, S11A, B). Moreover, the α-helical domains of Nup145C and Sec31 have completely different folds and topologies, yet both bind to overlapping regions on the bottom face of Sec13's β-propeller domain (Figure S11C). A comparison between the two structures reveals that the Sec13-Nup145C complex is overall much more compact (Figure S11C). The interfaces between Sec13 and the α-helical domains of Nup145C and Sec31 are unrelated, and the α-helical domains of either protein extend with different angles from the Sec13 β-propeller domain, resulting in a ~45° rotation with respect to their longest axes (Figure S11C).

Although both hetero-dimers form hetero-tetramers via their α-helical domains, their dimerization interfaces are different. While the Nup145C homo-dimerization interface appears rigid, the homo-dimerization interface of the Sec31 α-helical domain was proposed to form an adaptable hinge that would be required for the accommodation of various size vesicles (Fath et al., 2007). Both complexes oligomerize beyond the hetero-tetramer. Our crystallographic studies depict two Sec13-Nup145C hetero-tetramers that assemble into a hetero-octamer primarily via homo-dimerization of Sec13. In the case of the COPII complex, the higher-order oligomerization of its outer coat was deduced from fitting the Sec13-Sec31 hetero-tetramer into cryo-electron-microscopical density maps. It was proposed that lace-like cages are formed by an asymmetric homo-tetramerization of the N-terminal β-propeller domains of Sec31 (Fath

et al., 2007). A dimerization of the Sec13-Sec31 hetero-tetramer via Sec13, as has been described here for the Sec13-Nup145C complex, appears unlikely for the Sec13-Sec31 for steric reasons (Figure S11D). Hence, the function of Sec13 in either the NPC or the COPII complex has not been conserved. At this stage of structural analysis, the presence and the functional significance of Sec13 in the COPII complex remains a mystery.

The coat for the nuclear pore membrane does not form lace-like cages, as is the case for COPII and clathrin complexes (Bickford et al., 2004; Fath et al., 2007; Gurkan et al., 2006; Lederkremer et al., 2001; Salama et al., 1997), but instead forms a cylindrical layer that apposes the nuclear pore membrane. Unlike the vesicular transport cages, the nuclear pore membrane coat has evolved to recruit numerous additional proteins to transform the function of a mere membrane-coating module (Devos et al., 2004) into the bidirectional transport organelle that constitutes the nuclear pore complex.

EXPERIMENTAL PROCEDURES

Protein Expression and Purification

DNA fragments of yeast Nup145C (residues 1-711, and 125-555) were amplified by PCR and cloned into the pETDuet-1 (Novagen) expression vector using BamHI and NotI restriction sites. The resulting Nup145C fusion proteins contained an N-terminal 6-His tag. The amplified PCR fragments of human or yeast Sec13 (residues 1-322, and 1-316 of hSec13 and residues 1-297 of ySec13) were cloned into pET24b (Novagen) for the expression of untagged proteins. Using the same restriction sites, the full-length hSec13 (residues 1-322) fragment was cloned into a modified pET28a vector (Novagen) that contained a PreScission protease site directly after the N-terminal 6-His tag (Hoelz et al., 2003). DNA fragments encoding full-length yeast Seh1 (residues 1-349) and a C-terminally truncated yeast Nup85 fragment (residues 1-570) were cloned into the pETDuet-1 vector using BamHI-NotI and NdeI-XhoI restriction sites, respectively. The expression constructs are listed in Table S3.

For the expression of Sec13-Nup145C complexes, *E. coli* BL21-CodonPlus (DE3)-RIL cells (Stratagene) were co-transformed with the appropriate expression vectors, using the untagged Sec13 variants. Protein expression was carried out in LB medium and induced by the addition of 0.5 mM IPTG at 18°C for 16 hr. Cells were harvested by centrifugation and resuspended in a buffer containing 50 mM K-phosphate, pH 7.4, 150 mM NaCl, 5 mM β-mercaptoethanol, and protease inhibitor cocktail (Roche). The cells were lysed with a cell disrupter (Avestin), and the lysate was centrifuged for 90 min at 40,000 g. The lysate was then applied to a His-Select nickel column (Sigma) and eluted via an imidazole gradient. Fractions containing the Sec13-Nup145C complex were pooled and dialyzed against a buffer containing 20 mM HEPES, pH 7.4, 50 mM NaCl, and 3 mM DTT. The protein was purified over a HiTrap Q HP column (GE Healthcare) via a NaCl gradient and further purified over a 16/60 Superdex 200 column (GE Healthcare). Fractions containing the pure Sec13-Nup145C complex were pooled and concentrated to 12 mg/ml for crystallization.

The expression and purification of the Seh1-Nup85 complex and the various individual Sec13 proteins were carried out using an identical expression and purification protocol. The N-terminal 6-His tag of Sec13 was removed by PreScission protease cleavage for 36 hr.

Crystallization

Crystals of hSec13$^{1–316}$-Nup145C (12 mg/ml) were grown at 21°C in hanging drops containing 1 μl of the protein and 1 μl of a reservoir solution consisting of 16 % (w/v) PEG 3,350, 400 mM NaCl, 100 mM Na-K tartrate, and 100 mM BIS-TRIS, pH 7.7. Crystals grew in the orthorhombic space group $C222_1$ and the monoclinic space group C2. Both crystal forms

contain a Sec13-Nup145C hetero-octamer in the asymmetric unit. They grew to their maximum size, 1,000 × 300 × 200 μm, within 16 days. For cryoprotection, crystals were stabilized in 16 % (w/v) PEG 3,350, 400 mM NaCl, 100 mM Na-K tartrate, 100 mM BIS-TRIS, pH 7.7, and 22 % (v/v) glycerol and flash frozen in liquid nitrogen-cooled liquid propane. X-ray diffraction data were collected at the Advanced Light Source (ALS) and the National Synchrotron Light Source (NSLS). X-ray intensities were processed using HKL2000 (Otwinowski and Minor, 1997), and the CCP4 program package (CCP4, 1994) was used for subsequent calculations.

Structure Determination

Initial phases were determined using a $[Ta_6Br_{12}]^{2+}$ cluster derivative and MAD measurements of the orthorhombic crystals (Hoelz et al., 2003; Murakami et al., 2000; Stavropoulos et al., 2006). These phases were used to locate the heavy atom sites of sodium ethylmercurithiosalicylate (EMTS), potassium osmate (K_2OsO_4), and di-potassium tetrachloroplatinate (K_2PtCl_4)-derivatized and SeMet-labeled protein crystals (Figure S2). Combined phasing using isomorphous EMTS, K_2OsO_4, and SeMet MAD and native datasets was carried out in SHARP (La Fortelle and Bricogne, 1997), followed by density modification in DM (CCP4, 1994), with solvent flattening and histogram matching. This procedure yielded an interpretable electron density map of high quality. Phasing of the X-ray diffraction data derived from the monoclinic crystals was carried out independently with a similar phasing protocol, yielding an electron density map of comparable quality.

The initial model was built into the electron density map of the orthorhombic crystal form using O (Jones et al., 1991) and refined using CNS (Brünger et al., 1998). The final model was refined to a 3.0 Å resolution with an R_{work} of 24.7 % and an R_{free} of 28.9 %. No electron density was observed for the N-terminal 14 and C-terminal 12 residues, the residues 165 to 172 in Sec13, and the N-terminal 6 residues of Nup145C. These residues are presumed to be disordered and therefore have been omitted from the final model.

This final model was docked into the experimental electron density map of the monoclinic crystal form and refined using CNS. The final model was refined to a 3.15 Å resolution with an R_{work} of 24.7 % and an R_{free} of 29.2 %. The stereochemical quality of both final models was assessed with PROCHECK (Laskowski et al., 1993). There are no residues in the disallowed region of the Ramachandran plot. Data collection and refinement statistics are shown in Tables S1 and S2.

Multi-Angle Light Scattering

Protein at various concentrations was injected onto a Superdex 200 10/300 GL column equilibrated in a buffer containing 20 mM TRIS, pH 8.0, 100 mM NaCl, and 5 mM DTT. The chromatography system was coupled to an 18-angle light scattering detector (DAWN HELEOS) and a refractive index detector (Optilab rEX) (Wyatt Technology). Data were collected every 0.5 s at a flow rate of 0.4 ml/min. Data analysis was carried out using the program ASTRA, yielding the molar mass and mass distribution (polydispersity) of the sample (Wyatt, 1997).

Illustrations and Figures

Figures were generated using PyMOL (www.pymol.org). The molecular surfaces were calculated using MSMS (Sanner et al., 1996), and the electrostatic potential was calculated using APBS (Baker et al., 2001). Sequence alignments were generated using ClustalX (Jeanmougin et al., 1998) and colored with Alscript (Barton, 1993).

Supplementary Material

Refer to Web version on PubMed Central for supplementary material.

Acknowledgements

We thank E. Debler, O. Dreesen, I. Melcak, V. Nagy, J. Napetschnig, and A. Patke for discussions and comments on the manuscript, S. Etherton for help with editing the manuscript, and D. King for mass spectrometry analysis. In addition, we thank C. Ralston, B. Manjasetty, and W. Shi for support during data collection. N-terminal protein sequencing was performed by the Protein Center of the Rockefeller University. A.H. was supported by a grant from the Leukemia and Lymphoma Society.

References

Allen NP, Huang L, Burlingame A, Rexach M. Proteomic analysis of nucleoporin interacting proteins. J Biol Chem 2001;276:29268–29274. [PubMed: 11387327]

Bai SW, Rouquette J, Umeda M, Faigle W, Loew D, Sazer S, Doye V. The fission yeast Nup107-120 complex functionally interacts with the small GTPase Ran/Spi1 and is required for mRNA export, nuclear pore distribution, and proper cell division. Mol Cell Biol 2004;24:6379–6392. [PubMed: 15226438]

Baker NA, Sept D, Joseph S, Holst MJ, McCammon JA. Electrostatics of nanosystems: application to microtubules and the ribosome. Proc Natl Acad Sci USA 2001;98:10037–10041. [PubMed: 11517324]

Barton GJ. ALSCRIPT: a tool to format multiple sequence alignments. Protein Eng 1993;6:37–40. [PubMed: 8433969]

Beck M, Forster F, Ecke M, Plitzko JM, Melchior F, Gerisch G, Baumeister W, Medalia O. Nuclear pore complex structure and dynamics revealed by cryoelectron tomography. Science 2004;306:1387–1390. [PubMed: 15514115]

Belgareh N, Rabut G, Bai SW, van Overbeek M, Beaudouin J, Daigle N, Zatsepina OV, Pasteau F, Labas V, Fromont-Racine M, Ellenberg J, Doye V. An evolutionarily conserved NPC subcomplex, which redistributes in part to kinetochores in mammalian cells. J Cell Biol 2001;154:1147–1160. [PubMed: 11564755]

Berke IC, Boehmer T, Blobel G, Schwartz TU. Structural and functional analysis of Nup133 domains reveals modular building blocks of the nuclear pore complex. J Cell Biol 2004;167:591–597. [PubMed: 15557116]

Bickford LC, Mossessova E, Goldberg J. A structural view of the COPII vesicle coat. Curr Opin Struct Biol 2004;14:147–153. [PubMed: 15093828]

Boehmer T, Enninga J, Dales S, Blobel G, Zhong H. Depletion of a single nucleoporin, Nup107, prevents the assembly of a subset of nucleoporins into the nuclear pore complex. Proc Natl Acad Sci USA 2003;100:981–985. [PubMed: 12552102]

Brünger AT, et al. Crystallography & NMR system: a new software suite for macromolecular structure determination. Acta Crystallogr Sect D Biol Crystallogr 1998;54:905–921. [PubMed: 9757107]

CCP4. Collaborative Computational Project, Number 4, The CCP4 Suite: Programs for Protein Crystallography. Acta Crystallogr D 1994;50:760–763. [PubMed: 15299374]

Cronshaw JM, Krutchinsky AN, Zhang W, Chait BT, Matunis MJ. Proteomic analysis of the mammalian nuclear pore complex. J Cell Biol 2002;158:915–927. [PubMed: 12196509]

Devos D, Dokudovskaya S, Alber F, Williams R, Chait BT, Sali A, Rout MP. Components of coated vesicles and nuclear pore complexes share a common molecular architecture. PLoS Biol 2004;2:2085–2093.

Devos D, Dokudovskaya S, Williams R, Alber F, Eswar N, Chait BT, Rout MP, Sali A. Simple fold composition and modular architecture of the nuclear pore complex. Proc Natl Acad Sci USA 2006;103:2172–2177. [PubMed: 16461911]

Dockendorff TC, Heath CV, Goldstein AL, Snay CA, Cole CN. C-terminal truncations of the yeast nucleoporin Nup145p produce a rapid temperature-conditional mRNA export defect and alterations to nuclear structure. Mol Cell Biol 1997;17:906–920. [PubMed: 9001245]

Drin G, Casella JF, Gautier R, Boehmer T, Schwartz TU, Antonny B. A general amphipathic alpha-helical motif for sensing membrane curvature. Nat Struct Mol Biol 2007;14:138–146. [PubMed: 17220896]

Fahrenkrog B, Koser J, Aebi U. The nuclear pore complex: a jack of all trades? Trends Biochem Sci 2004;29:175–182. [PubMed: 15082311]

Fath S, Mancias JD, Bi X, Goldberg J. Structure and organization of coat proteins in the COPII cage. Cell 2007;129:1325–1336. [PubMed: 17604721]

Fontoura BM, Blobel G, Matunis MJ. A conserved biogenesis pathway for nucleoporins: proteolytic processing of a 186-kilodalton precursor generates Nup98 and the novel nucleoporin, Nup96. J Cell Biol 1999;144:1097–1112. [PubMed: 10087256]

Glavy JS, Krutchinsky AN, Cristea IM, Berke IC, Boehmer T, Blobel G, Chait BT. Cell-cycle-dependent phosphorylation of the nuclear pore Nup107-160 subcomplex. Proc Natl Acad Sci USA 2007;104:3811–3816. [PubMed: 17360435]

Gurkan C, Stagg SM, Lapointe P, Balch WE. The COPII cage: unifying principles of vesicle coat assembly. Nat Rev Mol Cell Biol 2006;7:727–738. [PubMed: 16990852]

Hoelz A, Blobel G. Cell biology: popping out of the nucleus. Nature 2004;432:815–816. [PubMed: 15602540]

Hoelz A, Nairn AC, Kuriyan J. Crystal structure of a tetradecameric assembly of the association domain of Ca2+/calmodulin-dependent kinase II. Mol Cell 2003;11:1241–1251. [PubMed: 12769848]

Jeanmougin F, Thompson JD, Guoy M, Higgins DG, Gibson TJ. Multiple sequence alignment with Clustal X. Trends Biochem 1998;23:403–405.

Jones TA, Zou JY, Cowan SW, Kjeldgaard M. Improved methods for building protein models in electron density maps and the location of errors in these models. Acta Crysallogr Sect A Found Crystallogr 1991;47:110–119.

King MC, Lusk CP, Blobel G. Karyopherin-mediated import of integral inner nuclear membrane proteins. Nature 2006;442:1003–1007. [PubMed: 16929305]

Krissinel, E.; Henrick, K. Detection of Protein Assemblies in Crystals. In: Berthold, MR., et al., editors. CompLife. Springer-Verlag; Berlin Heidelberg: 2005. p. 163-174.

La Fortelle ED, Bricogne G. Maximum-likelihood heavy-atom parameter refinement in the MIR and MAD methods. Methods Enzymol 1997;276:476–494.

Laskowski RA, MacArthur MW, Moss DS, Thornton JM. PROCHECK: a program to check the stereochemical quality of protein structures. J Appl Crystallogr 1993;26:283–291.

Lederkremer GZ, Cheng Y, Petre BM, Vogan E, Springer S, Schekman R, Walz T, Kirchhausen T. Structure of the Sec23p/24p and Sec13p/31p complexes of COPII. Proc Natl Acad Sci USA 2001;98:10704–10709. [PubMed: 11535824]

Loiodice I, Alves A, Rabut G, Van Overbeek M, Ellenberg J, Sibarita JB, Doye V. The entire Nup107-160 complex, including three new members, is targeted as one entity to kinetochores in mitosis. Mol Biol Cell 2004;15:3333–3344. [PubMed: 15146057]

Lutzmann M, Kunze R, Buerer A, Aebi U, Hurt E. Modular self-assembly of a Y-shaped multiprotein complex from seven nucleoporins. EMBO J 2002;21:387–397. [PubMed: 11823431]

Lutzmann M, Kunze R, Stangl K, Stelter P, Toth KF, Bottcher B, Hurt E. Reconstitution of Nup157 and Nup145N into the Nup84 complex. J Biol Chem 2005;280:18442–18451. [PubMed: 15741174]

Melcak I, Hoelz A, Blobel G. Structure of Nup58/45 suggests flexible nuclear pore diameter by intermolecular sliding. Science 2007;315:1729–1732. [PubMed: 17379812]

Murakami KS, Masuda S, Campbell EA, Muzzin O, Darst SA. Structural basis of transcription initiation: an RNA polymerase holoenzyme-DNA complex. Science 2000;296:1285–1290. [PubMed: 12016307]

Otwinowski Z, Minor W. Processing of X-Ray diffraction data collected in oscillation mode. Methods Enzymol 1997;276:307–326.

Pemberton LF, Paschal BM. Mechanisms of receptor-mediated nuclear import and nuclear export. Traffic 2005;6:187–198. [PubMed: 15702987]

Reichelt R, Holzenburg A, Buhle EL Jr, Jarnik M, Engel A, Aebi U. Correlation between structure and mass distribution of the nuclear pore complex and of distinct pore complex components. J Cell Biol 1990;110:883–894. [PubMed: 2324201]

Rout MP, Aitchison JD, Suprapto A, Hjertaas K, Zhao Y, Chait BT. The yeast nuclear pore complex: composition, architecture, and transport mechanism. J Cell Biol 2000;148:635–651. [PubMed: 10684247]

Salama NR, Chuang JS, Schekman RW. Sec31 encodes an essential component of the COPII coat required for transport vesicle budding from the endoplasmic reticulum. Mol Biol Cell 1997;8:205–217. [PubMed: 9190202]

Sanner MF, Olson AJ, Spehner JC. Reduced surface: an efficient way to compute molecular surfaces. Biopolymers 1996;38:305–320. [PubMed: 8906967]

Saxena K, Gaitatzes C, Walsh MT, Eck M, Neer EJ, Smith TF. Analysis of the physical properties and molecular modeling of Sec13: A WD repeat protein involved in vesicular traffic. Biochemistry 1996;35:15215–15221. [PubMed: 8952469]

Siniossoglou S, Lutzmann M, Santos-Rosa H, Leonard K, Mueller S, Aebi U, Hurt E. Structure and assembly of the Nup84p complex. J Cell Biol 2000;149:41–54. [PubMed: 10747086]

Siniossoglou S, Wimmer C, Rieger M, Doye V, Tekotte H, Weise C, Emig S, Segref A, Hurt EC. A novel complex of nucleoporins, which includes Sec13p and a Sec13p homolog, is essential for normal nuclear pores. Cell 1996;84:265–275. [PubMed: 8565072]

Suntharalingam M, Wente SR. Peering through the pore: nuclear pore complex structure, assembly, and function. Dev Cell 2003;4:775–789. [PubMed: 12791264]

Stavropoulos P, Blobel G, Hoelz A. Crystal structure and mechanism of human lysine-specific demethylase-1. Nat Struct Mol Biol 2006;7:626–632. [PubMed: 16799558]

Teixeira MT, Siniossoglou S, Podtelejnikov S, Benichou JC, Mann M, Dujon B, Hurt E, Fabre E. Two functionally distinct domains generated by in vivo cleavage of Nup145p: a novel biogenesis pathway for nucleoporins. EMBO J 1997;16:5086–5097. [PubMed: 9305650]

Vasu S, Shah S, Orjalo A, Park M, Fischer WH, Forbes DJ. Novel vertebrate nucleoporins Nup133 and Nup160 play a role in mRNA export. J Cell Biol 2001;155:339–354. [PubMed: 11684705]

Walther TC, Alves A, Pickersgill H, Loiodice I, Hetzer M, Galy V, Hulsmann BB, Kocher T, Wilm M, Allen T, Mattaj IW, Doye V. The conserved Nup107-160 complex is critical for nuclear pore complex assembly. Cell 2003;113:195–206. [PubMed: 12705868]

Wyatt PJ. Multiangle light scattering: the basic tool for macromolecular characterization. Instrum Sci Technol 1997;25:1–18.

Yang Q, Rout MP, Akey CW. Three-dimensional architecture of the isolated yeast nuclear pore complex: functional and evolutionary implications. Mol Cell 1998;1:223–234. [PubMed: 9659919]

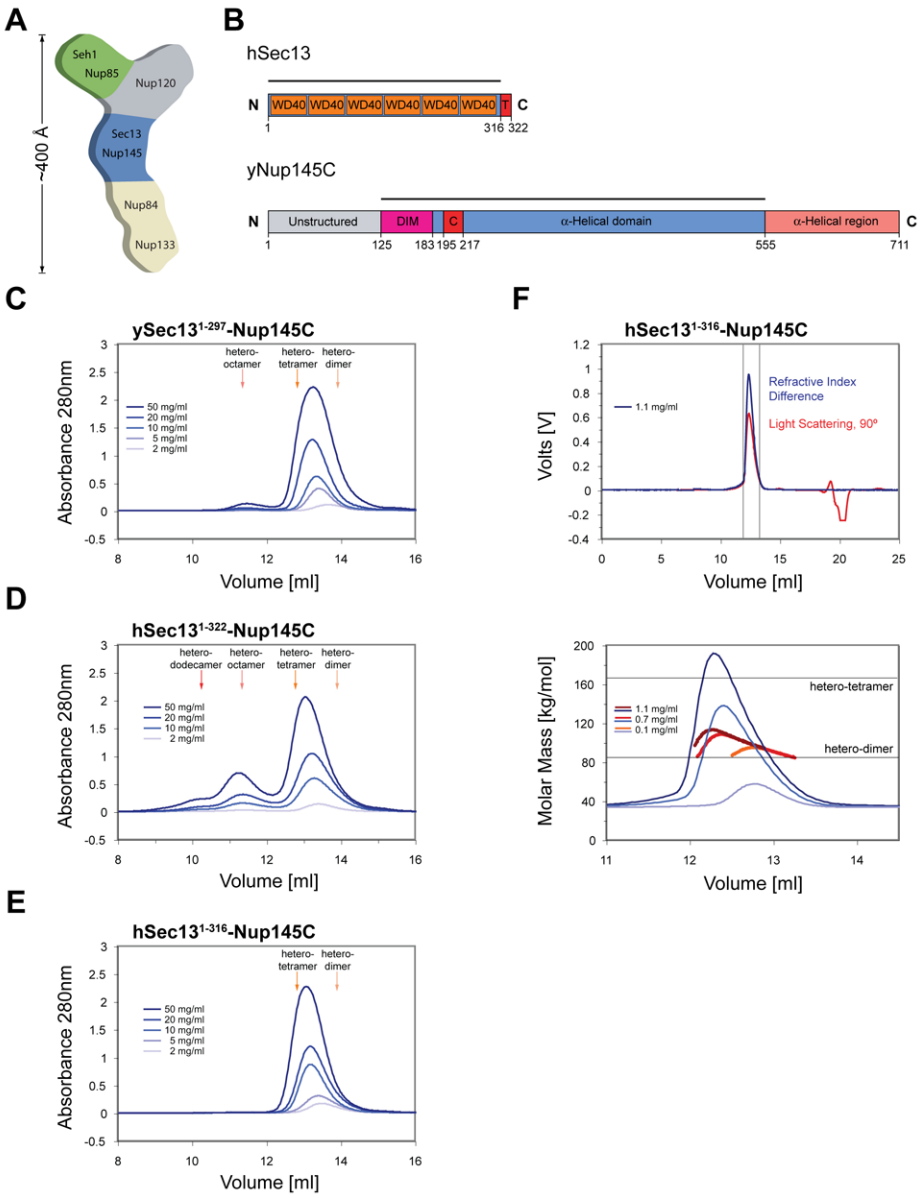

Figure 1. Organization and Dynamic Behavior of the Sec13-Nup145C Complex

(**A**) Schematic representation of the heptameric complex and the approximate localization of its seven nups (Lutzmann et al., 2002). (**B**) Domain structures of human Sec13 and yeast Nup145C. For Sec13, the WD40 repeats (orange), the C-terminal tail (T) (red), and the numbering relative to human Sec13 are indicated. For Nup145C, the unstructured N-terminal region (gray), the domain invasion motif (DIM) (purple), the αB-αC connector (C) (red), the α-helical domain (blue), and the C-terminal α-helical region (orange) are indicated. The numbering is relative to the yeast Nup145C. The bars above the domain structures of both proteins mark the crystallized fragments and are referred to as the Sec13-Nup145C complex. Gel filtration profiles of (**C**) the ySec13-Nup145C complex, (**D**) the hSec13$^{1–322}$-Nup145C complex, and (**E**) the C-terminally truncated hSec13$^{1–316}$-Nup145C complex. All proteins were injected at the indicated concentrations. The predicted elution positions for the various assembly states of the Sec13-Nup145C complexes are shown and have been determined using molecular weight standards. (**F**) Multi-angle light scattering analysis of the hSec13$^{1–316}$-

Nup145C complex. The black bars on each side of the peak delimit the data points used for further analysis (upper panel). Molecular weights were determined by light scattering at the three indicated protein concentrations (lower panel). The complex forms a concentration-dependent, polydisperse dynamic equilibrium between hetero-dimeric and hetero-tetrameric assemblies in solution.

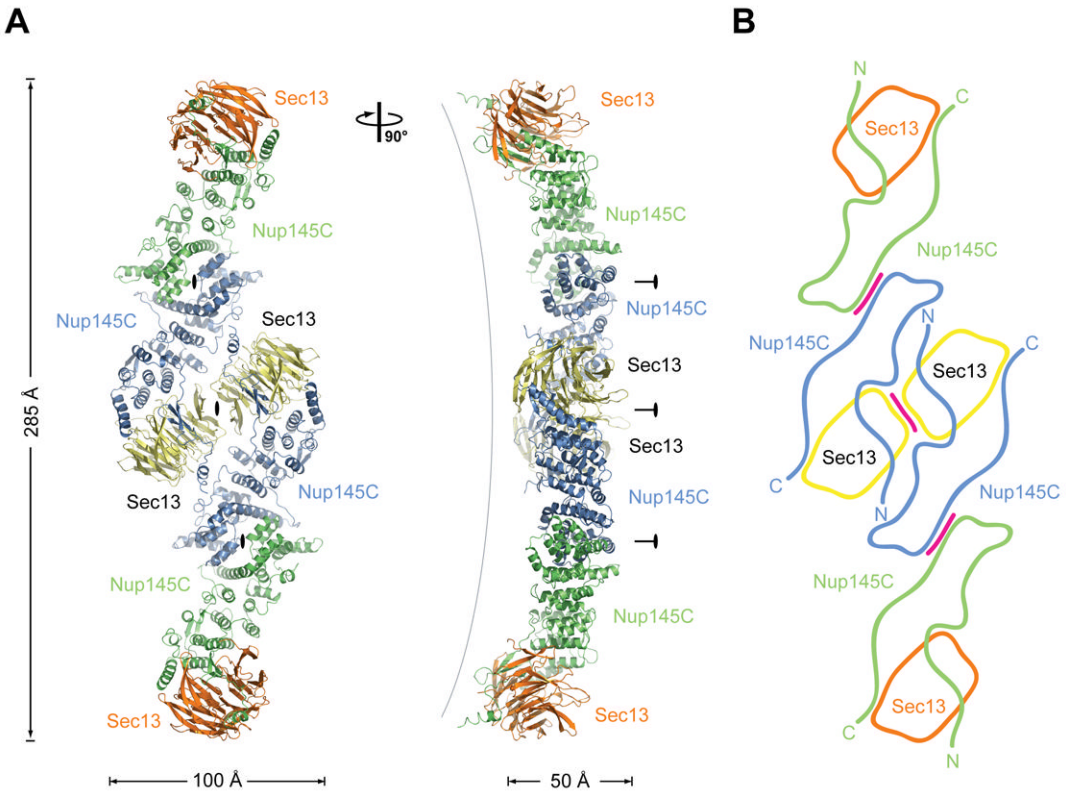

Figure 2. Overview of the Structure of the Sec13-Nup145C Hetero-Octamer

(**A**) Ribbon representation of the Sec13-Nup145C hetero-octamer, showing Sec13 in yellow and orange and Nup145C in green and blue. A 90° rotated view is shown on the right. The three pseudo-two-fold axes (black ovals) that run through the hetero-octamer and the overall dimensions are indicated. The Sec13-Nup145C hetero-octamer forms a slightly bent rod. (**B**) Schematic representation of the Sec13-Nup145C hetero-octamer. Magenta lines indicate interaction surfaces.

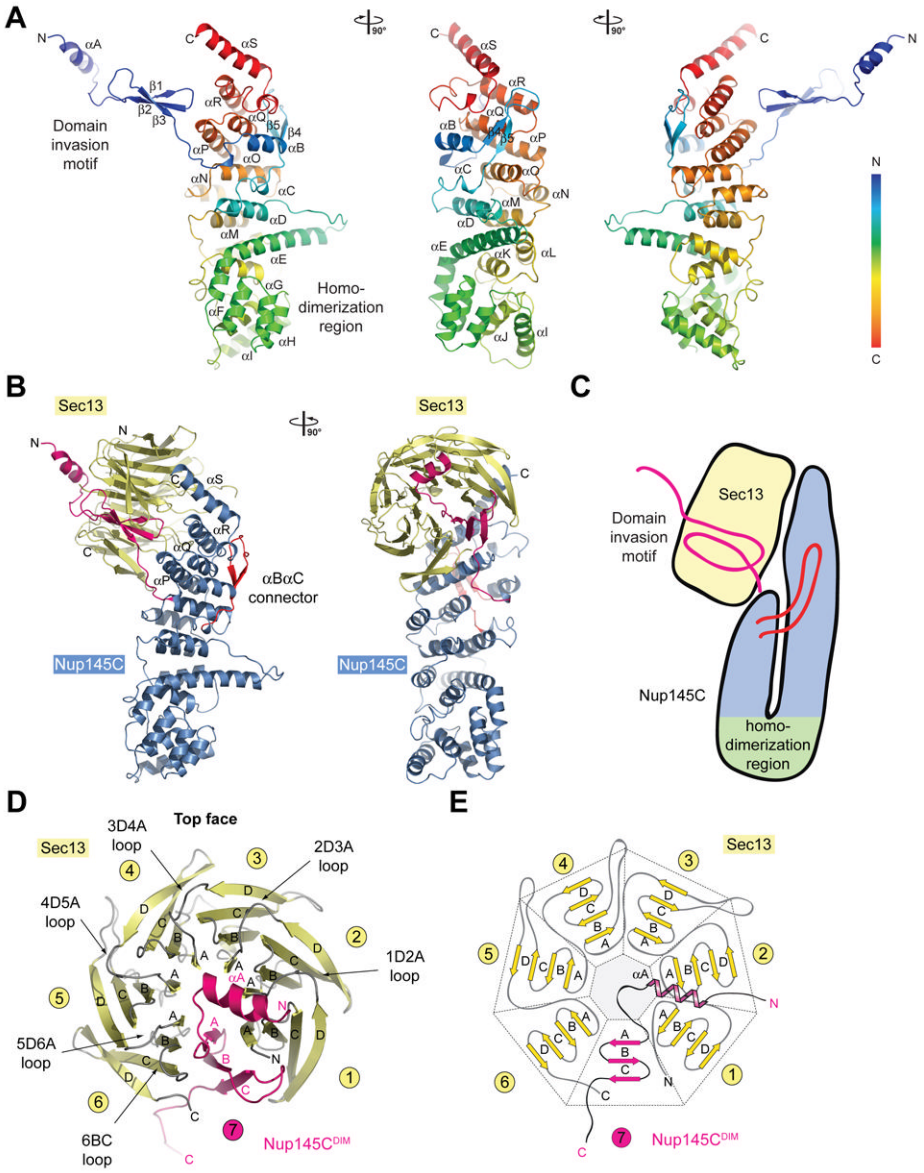

Figure 3. The Interaction of the Nup145C α-Helical Domain with the Sec13 β-Propeller

(**A**) The ribbon representation of the Nup145C structure is shown in rainbow colors along the polypeptide chain from the N- to the C-terminus. The N-terminal domain invasion motif (DIM), the C-terminal α-helical domain, and their secondary structure elements are indicated. (**B**) The structure of the Sec13-Nup145C hetero-dimer. The Nup145C^{DIM} (magenta), the Nup145C α-helical domain (blue), the Nup145C αB-αC connector segment (red), and the Sec13 β-propeller (yellow) are indicated; a 90° rotated view is shown on the right. (**C**) Schematic representation of the Sec13-Nup145C interaction. (**D**) The β-propeller domain of Sec13 in complex with the Nup145C^{DIM}. Sec13 is shown in yellow, and the six blades are indicated. The Nup145C^{DIM} forms a three-stranded seventh blade, complementing the Sec13 β-propeller domain. (**E**) Schematic representation of the Sec13 β-propeller and its interaction with the Nup145C^{DIM}.

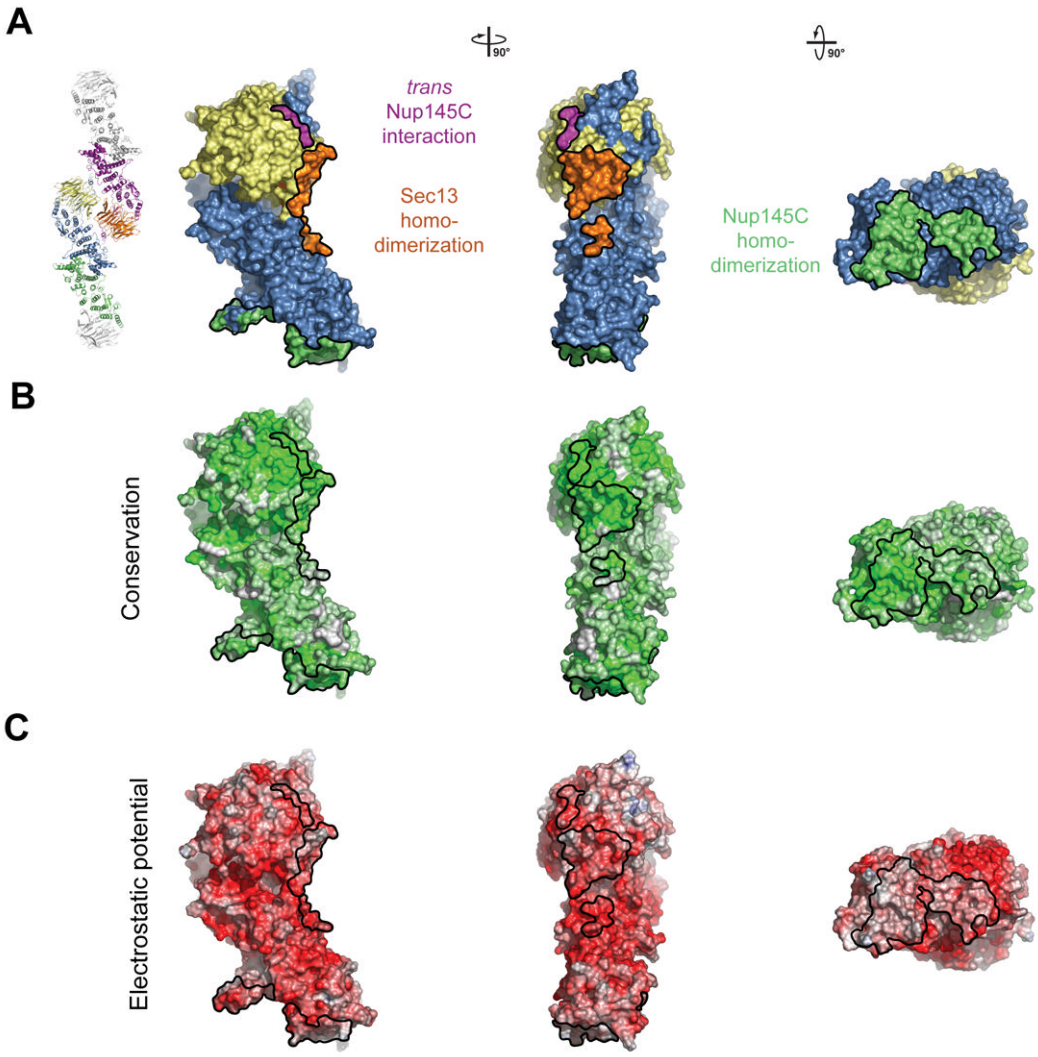

Figure 4. Surface Properties of the Sec13-Nup145C Hetero-Dimer

(**A**) Surface rendition of the Sec13-Nup145C complex. The surface is colored according to the proteins (Sec13, yellow; Nup145C, blue) and their participation in various interactions (Sec13 from the adjacent complex, orange; Nup145C from the adjacent complex, purple; Nup145C homo-dimerization, green). (**B**) Nup145C is colored according to sequence conservation, from 40 % similarity (white) to 100 % identity (green). (**C**) Surface rendition of Nup145C, colored according to the electrostatic potential, from red (−10 k_BT/e) to blue (+10 k_BT/e).

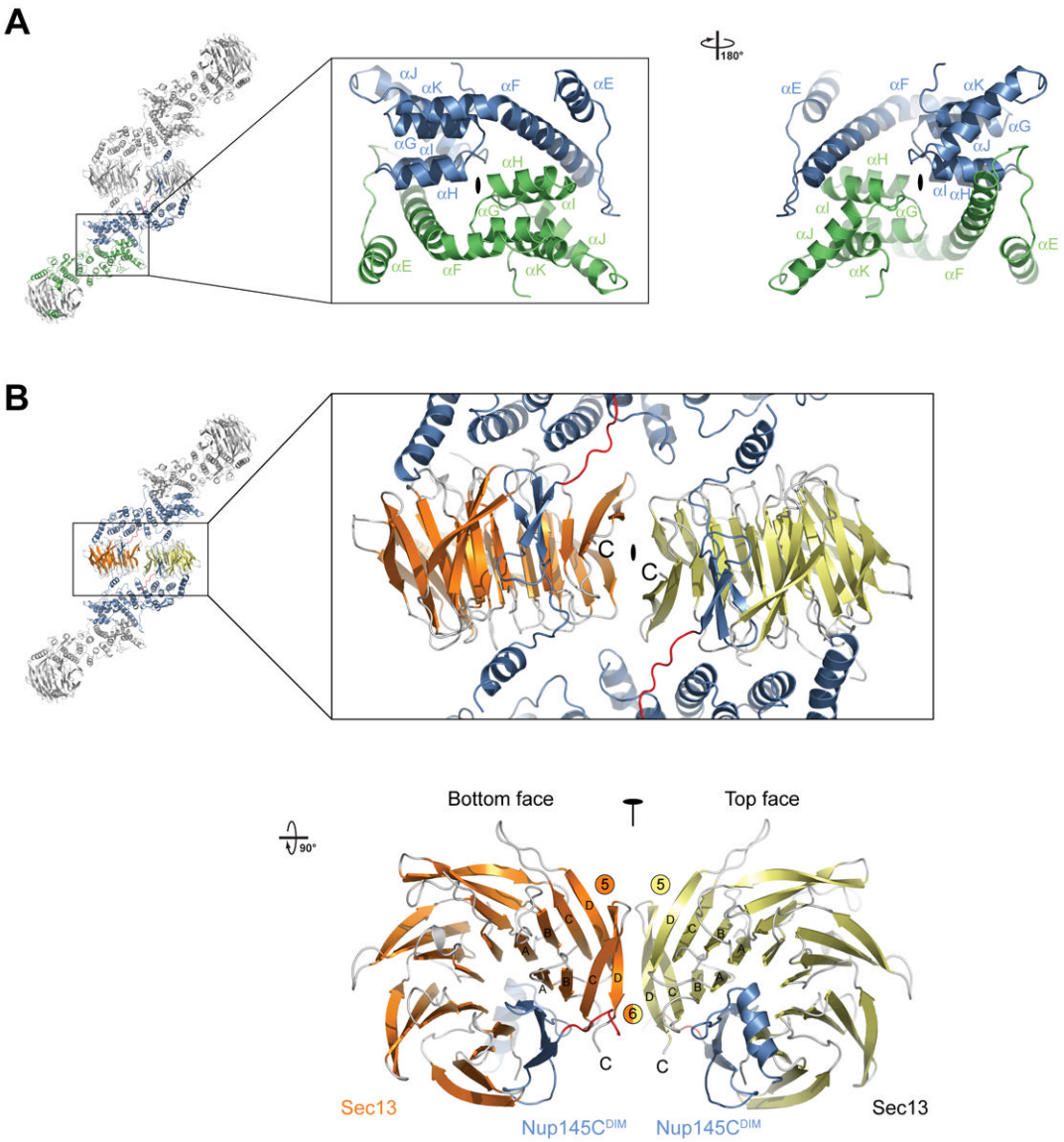

Figure 5. The Assembly of the Sec13-Nup145C Hetero-Octamer

(**A**) Ribbon representation of the dimerization of the Nup145C α-helical domain. For clarity, only the two interacting Nup145C protomers in the hetero-octamer are colored (green and blue). The centrally located α-helices that facilitate the homo-dimerization of Nup145C are indicated. A 180° rotated view is shown on the right. (**B**) The dimerization interface located in the center of the Sec13-Nup145C hetero-octamer. The two Sec13 β-propeller domains (orange and yellow) and two Nup145C molecules (blue) are colored. The two Sec13 C-termini (the last ordered residue is Val304) are indicated and are only ~10 Å apart. A 90° rotated view is shown below. The locations of the pseudo-two-fold axes of symmetry that run through both interfaces are indicated (black ovals).

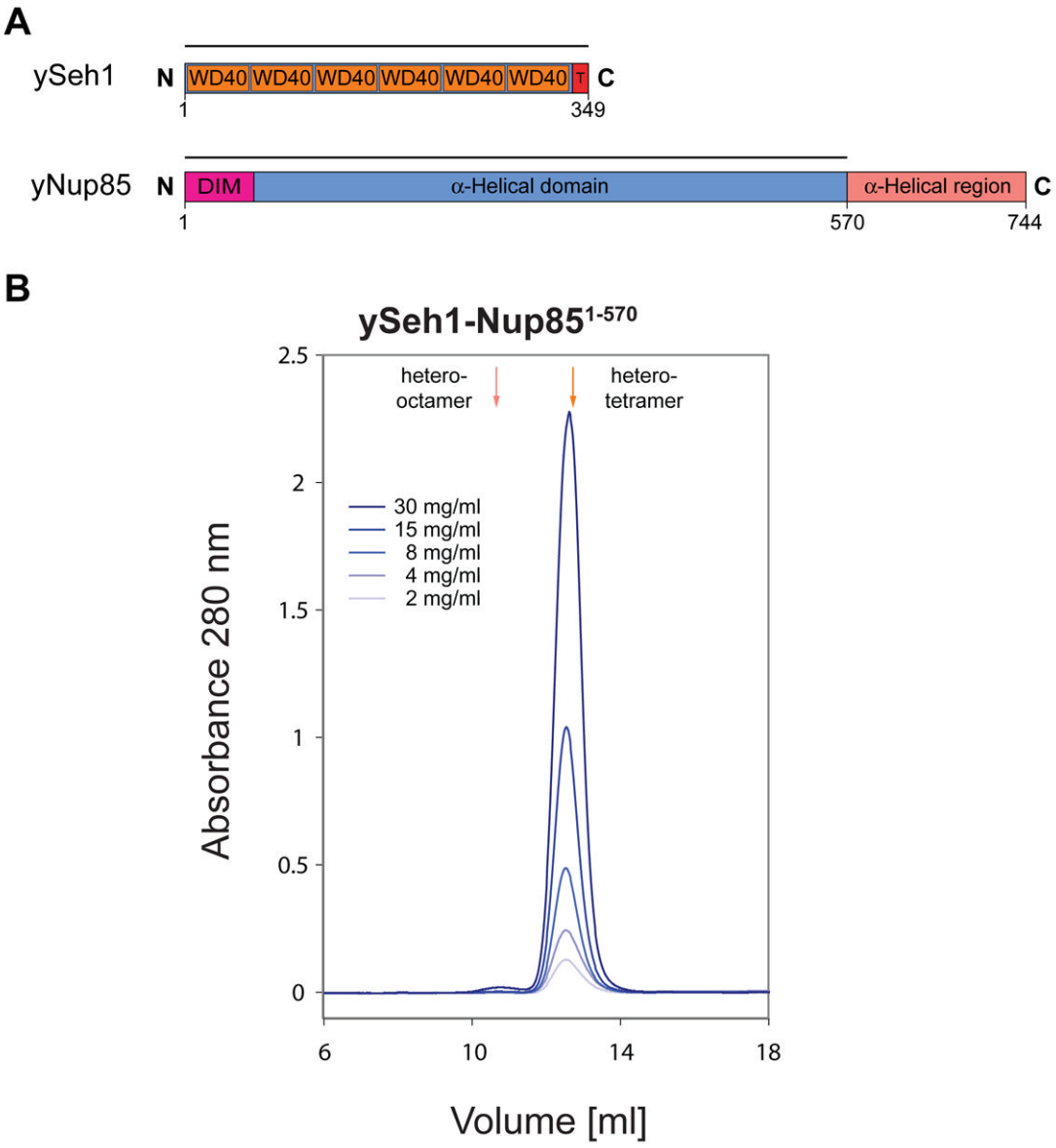

Figure 6. Biochemical Characterization of the Seh1-Nup85 Complex

(**A**) Domain structures of yeast Seh1 and yeast Nup85. For Seh1, the six WD40 repeats (orange), the C-terminal tail (T) (red), and the numbering are indicated. For Nup85, the predicted domain invasion motif (DIM) (magenta), the ⟨-helical domain (blue), and the C-terminal ⟨-helical region (orange) are indicated. The bars above the domain structures of both proteins mark the expressed fragments. (**B**) Gel filtration profiles of the yeast Seh1-Nup85 complex. The Seh1-Nup85 complex was injected at the indicated protein concentrations. The predicted elution positions for heter-tetrameric and hetero-octameric Seh1-Nup85 complexes are shown and have been determined using molecular weight standards.

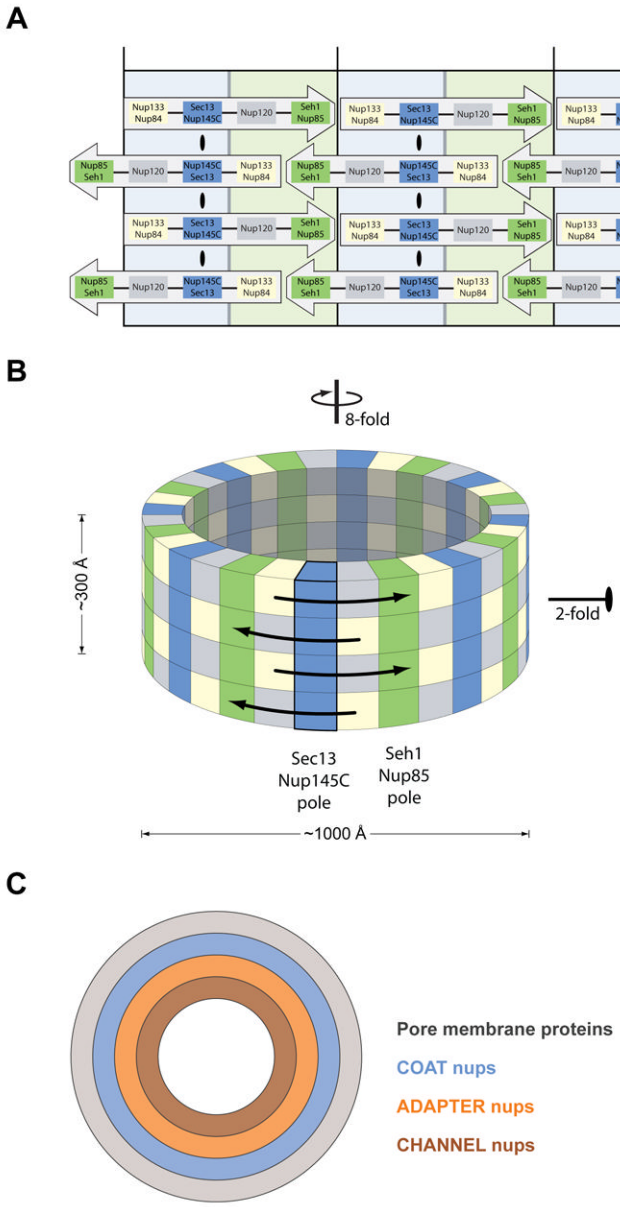

Figure 7. Model for the Architecture of the Symmetric NPC Core

(**A**, **B**) Eight Heptamers are circumferentially arranged in a head-to-tail fashion in four stacked rings. The Sec13-Nup145C and Seh1-Nup85 hetero-octamers serve as vertical poles connecting the four rings, thereby forming a scaffold. The poles are connected through their interaction with the remaining nups of the heptameric complex. Based on the two-fold axes of symmetry in the Sec13-Nup145C hetero-octamer, the heptameric complex rings are stacked with opposite directionality. (**C**) The symmetric core of the NPC is schematically represented as a series of concentric cylinders as discussed in the text. Each of the four envisaged cylinders would contain the principal mass of the following proteins: integral pore membrane proteins (Pom152, Pom34, and Ndc1), coat nups (Seh1, Nup85, Nup120, Sec13, Nup145C, Nup84, and Nup133), adapter nups (Nic96, Nup192, Nup188, Nup157, and Nup170), and the channel nups (Nsp1, Nup49, and Nup57).